






Research Article

Acridine-2,4-Dinitrophenyl Hydrazone Conjugated Silver Nanoparticles as an Efficient Sensor for Quantification of Mercury in Tap Water

Imdad Ali,¹ Ibanga Okon Isaac,¹ Mahmood Ahmed ,² Farid Ahmed,¹ Farhat Ikram,³ Muhammad Ateeq,⁴ Rima D. Alharthy ,⁵ Muhammad Imran Malik ,¹ Abdul Hameed ,^{1,6} and Muhammad Raza Shah ¹

¹H.E.J. Research Institute of Chemistry, International Center for Chemical and Biological Sciences, University of Karachi, Karachi 74200, Pakistan

²Department of Chemistry, Division of Science and Technology, University of Education, College Road, Lahore-, Pakistan

³Department of Chemistry, N.E.D. University of Engineering and Technology, Karachi 75270, Pakistan

⁴Department of Chemistry, Abdul Wali Khan University, Mardan, Pakistan

⁵Chemistry Department, Faculty of Science and Arts, King Abdulaziz University, Rabigh 21911, Saudi Arabia

⁶Department of Chemistry, University of Sahiwal, Sahiwal 57000, Pakistan

Correspondence should be addressed to Mahmood Ahmed; mahmoodresearchscholar@gmail.com, Abdul Hameed; abdul_hameed8@hotmail.com, and Muhammad Raza Shah; raza.shah@iccs.edu

Received 14 December 2021; Revised 26 February 2022; Accepted 9 March 2022; Published 26 March 2022

Academic Editor: Andrea Mastinu

Copyright © 2022 Imdad Ali et al. This is an open access article distributed under the Creative Commons Attribution License, which permits unrestricted use, distribution, and reproduction in any medium, provided the original work is properly cited.

Excretion of heavy metals especially mercury (Hg^{2+}) from the industries into the environment becomes a major global problem. In this context, mercury is a highly dangerous metal which poses serious impact on human health. In the present study, acridine-(ACR-) based silver nanoparticles (ACR-AgNPs) were prepared and employed as a nanosensor for effective detection and quantification of Hg^{2+} in tap water. Conjugation between ACR-based coating agent and silver was examined by UV-visible and FT-IR spectroscopy, while morphology and particle size were determined through atomic force microscopy (AFM), dynamic light scattering (DLS), and scanning electron microscopy (SEM). Furthermore, sensing behavior of nanosensor for metal ions was evaluated by mixing different metals such as Mn^{2+} , Ni^{2+} , Ba^{2+} , Mg^{2+} , Cr^{3+} , Pb^{2+} , Pd^{2+} , Al^{3+} , Sn^{2+} , Fe^{2+} , Co^{2+} , Cu^{2+} , Fe^{3+} , Cd^{2+} , and Hg^{2+} with ACR-AgNPs. Among all the added metal ions, only Hg^{2+} resulted in significant quenching in the absorption intensity of ACR-AgNPs. The limit of detection of the ACR-AgNP-based nanosensor was found to be $1.65 \mu\text{M}$ in a wide pH range (1-14). The proposed mercury sensor worked efficiently in the presence of other interfering agents such as other metal ions. Therefore, the synthesized ACR-AgNPs have proved to be an efficient and robust nanosensor for quantitative detection of Hg^{2+} in real sample analysis such as tap water. The proposed method does not require expensive instrumentation and trained manpower.

1. Introduction

The excretion of heavy metal from the industries in the environment has become a major global problem. Mercury (Hg^{2+}) is one of highly toxic pollutant which is found in soil, water, and air [1]. It is a highly dangerous metal and causes serious health problems to humans and animals. Its direct contact with eyes results in vision loss.

The human central nervous system is badly affected by action of Hg^{2+} ions, if it presents in the blood. It also induces lung problem, the person feel breathing problem that leads to kidney failure and to ultimate death [2–8]. It has been estimated that the total amount of Hg added from industries into the environment is about 5,000–8,000 metric tons per year [9, 10]. Various techniques have been employed for detection of Hg^{2+} ions in the soil,

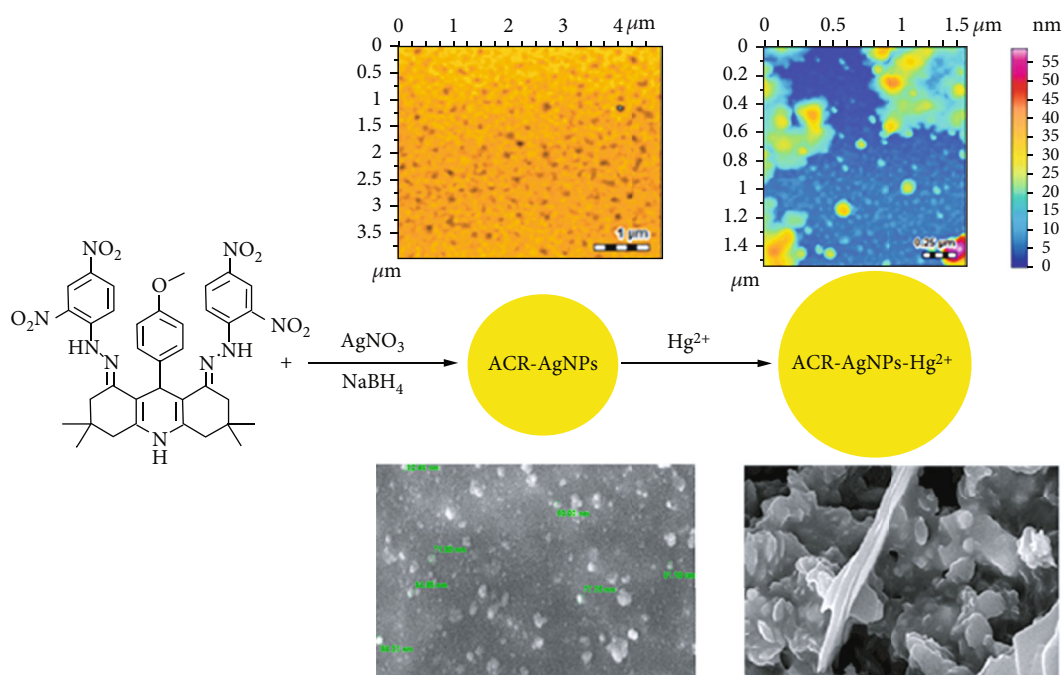


FIGURE 1: Graphical presentation of present study.

water, and even in the air that include atomic absorption or emission spectroscopy (AAS/AES) [11, 12], X-ray absorption spectroscopy (XAS) [13], inductively coupled plasma mass spectrometry (ICP-MS) [8], and atomic fluorescence spectrometry (AFS) [14]. Previous methods are difficult, costly, require expensive instruments, and also expertise of manpower to run these instruments. Therefore, it is necessary to develop an easy, economic, selective, and sensitive method for detection of mercury in the environmental samples. Recently, fluorescent and colorimetric sensors are found to be easily approachable, and facile method for the detection of environmentally pollutant metal ions (Hg^{2+} ions) [15–19]. Due to presence of electronic configuration of d10 orbital of mercury, there is no spectral signature that inhibits its practical applications [20–22]. However, due to having this unique feature (Hg^{2+} ions), the nanosensor has great optical response to detect Hg^{2+} ions present in biological samples or in the environment [22–24]. The nanosensors have remarkable ability to detect mercury ions (Hg^{2+}) even if it is present in the very small amounts. In this context, silver nanoparticles of chemosensors were synthesized which possess strong optical response in the spectral range of 400 to 480 nm. The addition of external substances in the AgNPs results in the spectral shift (bathochromic, hyperchromic, hypsochromic, and hypochromic) due to interaction between external species with silver nanoparticles [25–27]. Moreover, nanoparticles of silver are cheap, nontoxic, and environment friendly. Furthermore, these have great capability to detect the heavy metal ions (Hg^{2+} ions) and have high selectivity and sensitivity depending upon the nature of the used stabilizing agent. Various methods are present to synthesize AgNPs such as chemical reduction method, ion sputtering, and sol gel [28–30]. The abovementioned methods engage

harmful chemicals and also need high energy which may cause decomposition of the chemosensors [31, 32]. Due to the nontoxic nature and biological applications, the silver nanoparticles have great attention for the scientists, chemists, and pharmaceuticals [33–35]. Moreover, silver nanoparticles provide remarkable opportunity to detect the heavy metal ions, dyes, pesticides, fertilizers, bacteria, fungi, and drugs in the environmental and biological systems.

Acridines derived from anthracenes belong to the class of heterocyclic compounds [36]. It is formed when two rings fuse in a central position to a pyridine ring, also recognized as dibenzo-pyridine. Derivatives of acridine are well-known for their remarkable pharmaceutical and biological properties [37–39]. Interesting molecular structure of acridine derivatives raised our interest to explore their potential as sensors. Therefore, we targeted to prepare silver nanoparticles by using (1*E*,8*E*)-1,8-bis(2-(2,4-dinitrophenyl)hydrazono)-9-(4-methoxyphenyl)-3,3,6,6-tetramethyl-1,2,3,4,5,6,7,8,9,10-decahydroacridine (ACR) as stabilizer and to explore their potential for sensing Hg^{2+} in environmental samples. Different spectroscopic techniques were carried out for the characterization of acridine-based silver nanoparticles such as UV-visible and FT-IR spectroscopy, while morphology and particle size were observed through atomic force microscopy (AFM), dynamic light scattering (DLS), and scanning electron microscopy (SEM). The detection and quantification of mercury ions are the major target of current study (graphical description, Figure 1).

2. Methods and Material

2.1. Materials and Instrumentations. All the chemicals used were of analytical grade and were procured from Sigma

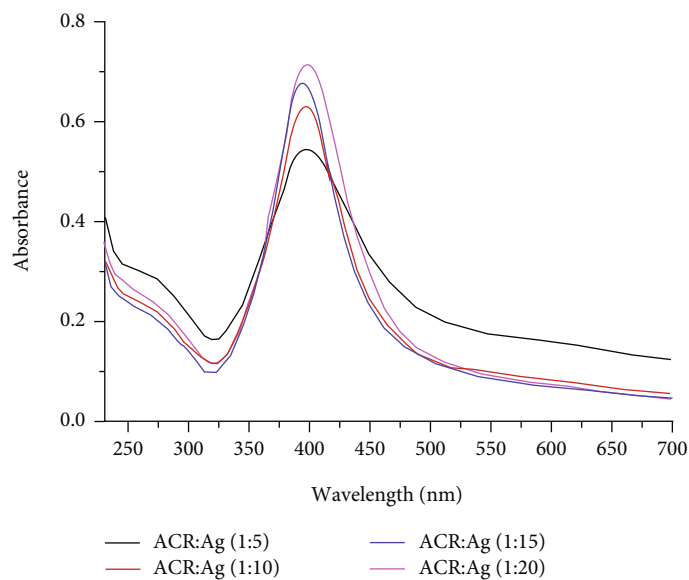


FIGURE 2: UV-visible spectra of acridine-coated silver nanoparticles (ACR-AgNPs).

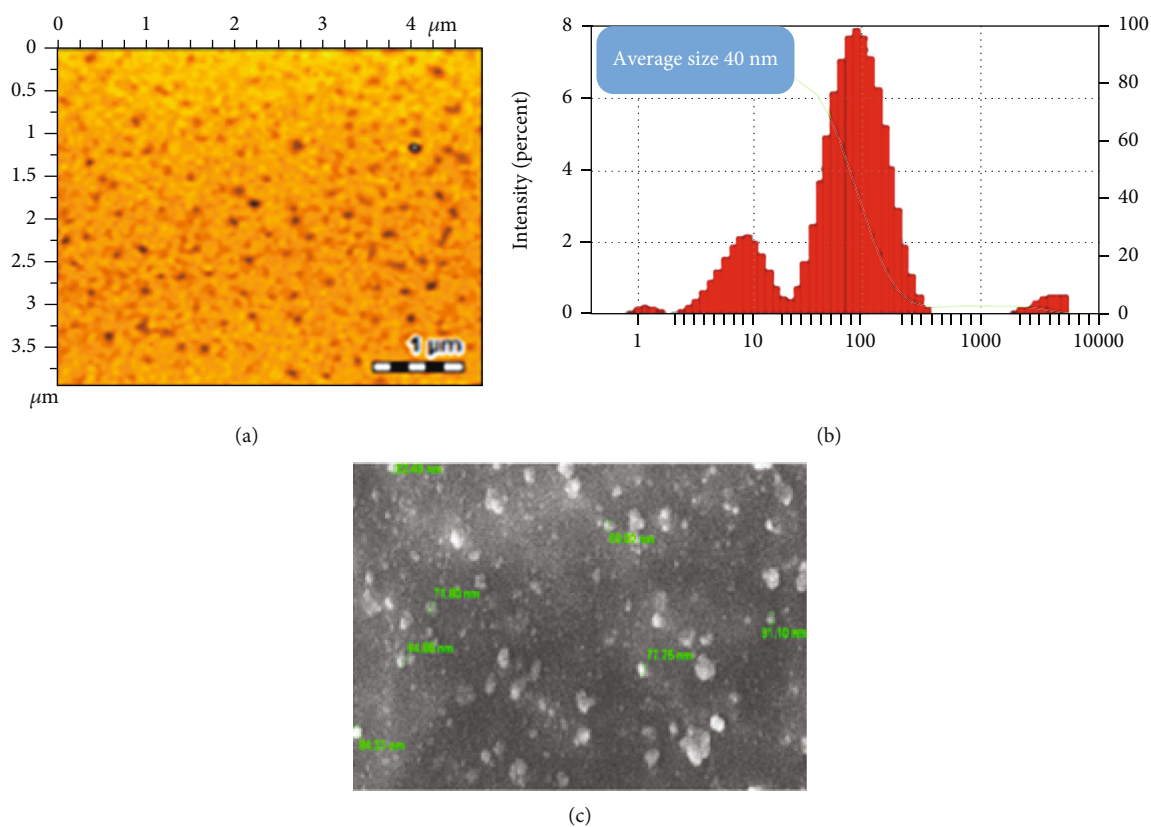


FIGURE 3: (a) Two-dimensional AFM images of ACR-AgNPs. (b) The percent intensity size distribution of ACR-AgNPs. (c) SEM image of ACR-AgNPs.

Aldrich. All the solvent used in this study were analytical grade and were purchased from Riedel-de Haen. The UV-visible spectroscopy was conducted on Shimadzu-240 Tokyo, Japan, having a one-centimeter quartz cuvette. The morphology of samples was determined with atomic force microscopy (Agilent-5500, USA). A diluted drop of

sample was put on the mica, air dried, and analyzed in contact mode. The average size and zeta potential were observed by zeta sizer. The measurement of pH of the sample was done through model 510 pH meter (Oakton, Eutech), having Ag/AgCl (reference) electrode and a glass (working) electrode.

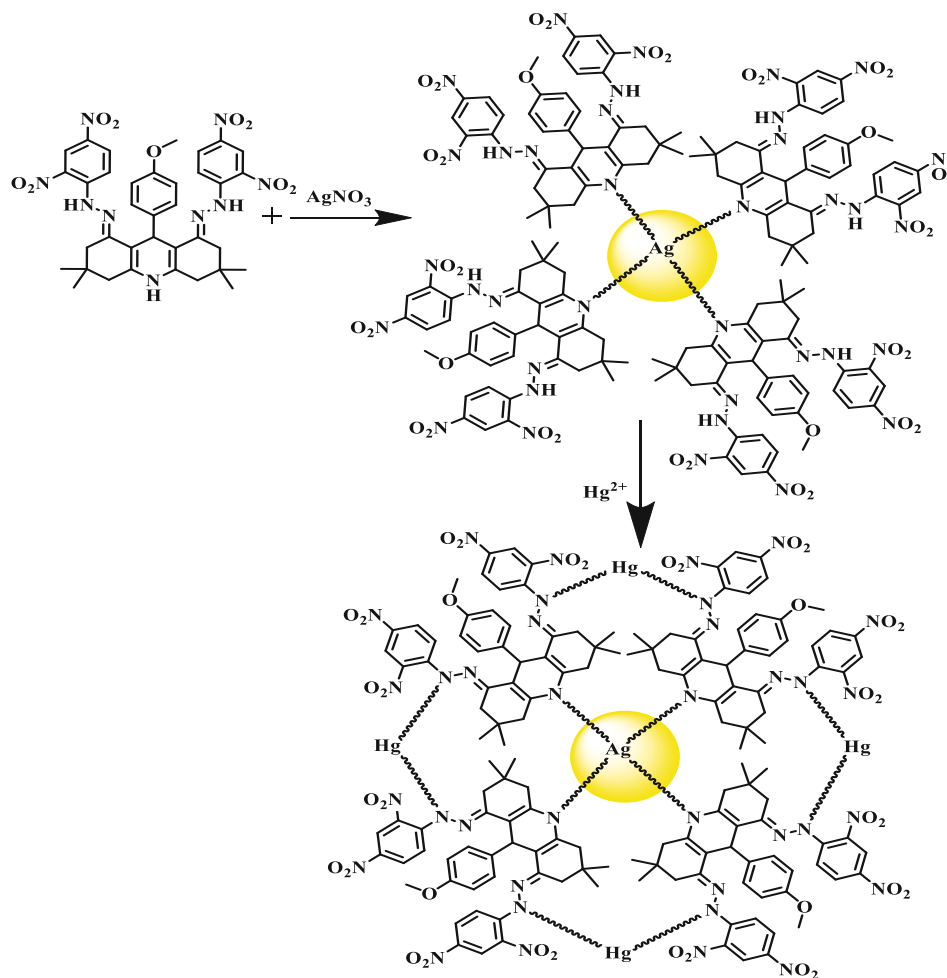


FIGURE 4: Schematic representation of nanoparticles synthesis and complexation with Hg^{2+} .

2.2. Synthesis and Characterization of ACR. (1*E*,8*E*)-1,8-bis(2-(2,4-dinitrophenyl)hydrazono)-9-(4-methoxyphenyl)-3,3,6,6-tetramethyl-1,2,3,4,5,6,7,8,9,10-decahydroacridine (ACR) was synthesized by mixing benzaldehyde, ammonium acetate, dimedone, and nickel (II) fluoride tetrahydrate (catalyst) in ethanol. After maintaining acidic medium by using acetic acid, hydrazine hydrate, phenyl isothiocyanate, and 2,4-dinitrophenyl hydrazine were added. Details of synthesis and characterization of ACR have been given in our recent publication [40].

2.3. Synthesis of ACR-AgNPs. ACR-AgNPs were synthesized by chemical reduction method using sodium borohydride as a reducing agent. Stock solution of silver nitrate (1 mM) was prepared in deionized water which was further diluted to 0.1 mM. A 1.0 mM solution of ACR was prepared in ethanol and further diluted up to 0.1 mM. To synthesize ACR conjugated silver nanoparticles (ACR-AgNPs), equimolar solutions of synthesized ACR (0.1 mM) and silver nitrate (0.1 mM) were mixed in several ratios (1:5, 1:10, 1:15, and 1:20) and stirred at room temperature for 10 minutes. After that, few drops (5-6) of NaBH_4 (4 mM) were added and resulted solution was stirred further. After 30 minutes

of continuous stirring, yellow color appears in the initially colorless solution indicating the formation of colloidal silver nanoparticles. The synthesized ACR-AgNPs were centrifuged at 12000 rpm for 12 min until pellets were obtained, after discarding supernatant followed by freeze drying to obtain solid ACR-AgNPs. The obtained nanoparticles were stored at 4°C for further use.

2.4. Morphological Analysis by AFM. For determination of particles size and surface morphology of the synthesized ACR-AgNPs. For the analysis of the complexation between ACR-AgNPs and Hg^{2+} , both the solutions were mixed in 1:1 ratio (v/v). For AFM sample preparation, 10 μL freshly prepared solution of ACR-AgNPs was placed on a cleaned mica disc and dried in air. After complete drying, AFM analysis was performed in tapping mode.

2.5. FTIR Analysis. FT-IR spectra in the range 400-4000 cm^{-1} were recorded by FT-IR 8900 Shimadzu using KBr disc. For FTIR analysis of ACR-AgNPs, 5 mg dried nanoparticles were mixed with a small amount of KBr powder and grounded to a fine disc. Similarly, 5 mg of ACR-AgNPs powder mixed with equal ratio with Hg^{2+} was mixed with a small

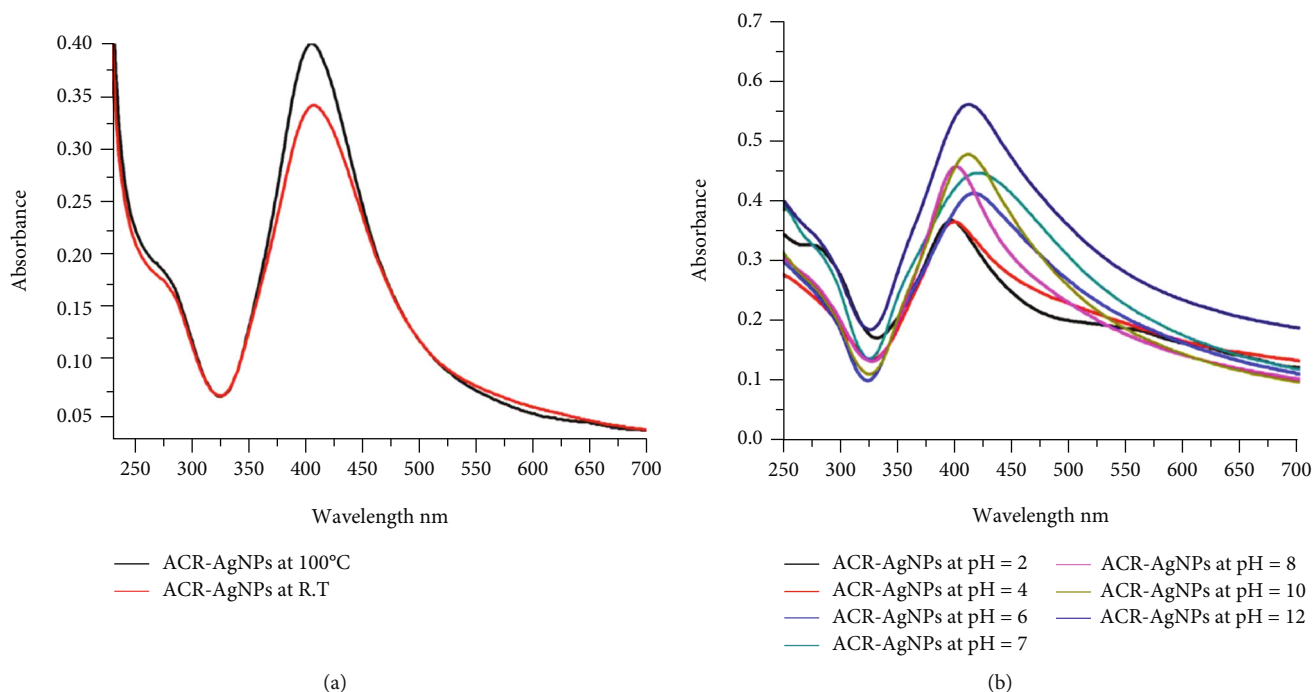


FIGURE 5: Stability of ACR-AgNPs. (a) Effect of temperature treatment. (b) Effect of pH on the stability of ACR-AgNPs.

amount of KBr and grounded to a fine disc. Thereafter, analysis was done by FT-IR 8900 Shimadzu, Japan.

2.6. General Methods for Sensing Experiments. The photo-physical potential of ACR-AgNPs towards metal ions was explored using UV-visible spectroscopy. For general screening experiments, 1.0 mL of freshly prepared ACR-AgNPs solution was mixed with various metal ions (100 μM), and changes in the absorption spectrum were recorded. For the determination of limit of detection for Hg^{2+} , concentration-dependent experiments were performed, various concentration of Hg^{2+} (5-100 μM) were treated with ACR-AgNPs. The limit of detection for Hg^{2+} was calculated using standard deviation of blank and slope of straight-line equation using following formula $\text{LOD} = 3.3 \times \text{S.D./Slope}$. For competitive analysis, several interfering metal ions were tested in presence of Hg^{2+} , and obtained results were compared with that of Hg^{2+} alone.

2.7. Spiking in Tap Water. 100 μM solution of mercury was prepared in laboratory tap water taken from the University of Karachi. The freshly prepared ACR-AgNPs were mixed with mercury solution of equal concentration and equal quantity prepared in tap water. UV-visible spectrum was recorded and compared with spectrum recorded in deionized water.

3. Results and Discussion

3.1. Synthesis of ACR-AgNPs. UV-visible spectra were recorded to finalize the suitable ratio for optimum stabilization of ACR-AgNPs. Spectral analysis showed that ACR to AgNO_3 ratio of 1:10, 1:15, and 1:20 gave a sharp peak as compared to the ratio 1:5 at 410 nm (Figure 2). Peak broad-

ness may lead to incorrect results as the addition of any interfering substance especially low concentration may not induce a significant response. Thus, ratio 1:20 was used for the synthesis of ACR-AgNPs because in this ratio the more nanoparticles are formed and the peak is sharp and of high intensity.

3.2. Characterization of ACR-AgNPs. The morphology and size of ACR-AgNPs were examined by two-dimensional and three-dimensional images obtained by atomic force microscopy (AFM), which showed spherical particles in the size range of 40 to 45 nm (Figure 3(a)). And also the SEM (scanning electron microscopy) analysis of the same revealed the spherical shape of the ACR-AgNPs having a size in similar range (Figure 3(c)).

Size distribution of ACR-AgNPs is examined through dynamic light scattering (DLS) in terms of percent intensity, ACR-AgNPs showed the average size of 40 nm and polydispersity index (PDI) of 0.556, Figure 3(b). FTIR spectra of ACR and ACR-AgNPs were recorded between 4000 and 500 cm^{-1} . Spectra showed prominent infrared absorbance peaks at 1618 cm^{-1} . Stretching vibration of carbon-carbon single and carbon-carbon double bond (aromatic) causes absorbance bands at 1585, 1618, 1477, and 1423 cm^{-1} . Asymmetric stretch of $-\text{C}-\text{O}-$ and CH_3 (bend) is observed at 1129 and 1253 cm^{-1} . Whereas peaks at 1511 and 1330 cm^{-1} indicate C-N and N-H stretching of aromatic amine. Stretching vibrations of secondary amine (NH) group of acridine showed a broadband at 3300 cm^{-1} while a sharp band appeared at 3644 cm^{-1} . In spectrum of acridine conjugated silver nanoparticles, the -N-H band shifted from 3300 cm^{-1} to 3443 cm^{-1} . These findings suggest that the secondary amine nitrogen of ACR takes part in the stabilization of silver nanoparticles (Figure 4) [41, 42].

3.3. Stability of ACR-AgNPs. Stability of nanoparticle under different conditions plays critical role in application of nanoparticles to the real samples. In order to determine the stability of newly synthesized ACR-AgNPs, different parameter was optimized such as pH of the medium and effect of temperature on the stability of nanoparticles. In order to determine the effect of temperature on the stability of nanoparticle, ACR-AgNPs were boiled to 100°C, cooled to room temperature, and spectra were recorded. As can be seen from Figure 5(a), ACR-AgNPs are found to be more stable after temperature treatment. The effect of pH on the stability of ACR-AgNPs was also optimized as shown in Figure 5(b). The newly prepared AgNPs stabilized by ACR were found to be highly stable in a wide range of pH (2-12).

3.4. ACR-AgNPs as Sensor. As a real target of this study, the effect of addition of commonly found ions/metal ions such as NH_4^+ , Mn^{2+} , Ni^{2+} , Ba^{2+} , Mg^{2+} , Cr^{3+} , Pb^{2+} , Pd^{2+} , Al^{3+} , Sn^{2+} , Fe^{2+} , Co^{2+} , Cu^{2+} , Fe^{3+} , Cd^{2+} , and Hg^{2+} in ACR-AgNPs is evaluated. UV-visible spectra of the ACR-AgNPs after addition of metal salt solutions (100 μM) in 1:1 ratio is recorded (Figure 6). Addition of mercury solution in ACR-AgNPs resulted in decrease in the absorbance intensity that could be linked to the binding of Hg^{2+} with the nitrogen of ACR-AgNPs by their lone pairs. As depicted in Figure 4 most probably, the Hg^{2+} forms stable complex with Schiff base nitrogen atom of ACR-AgNPs. After the complex formation with Hg^{2+} , the electronic environment of ACR-AgNPs is disrupted and consequently absorption intensity decreased significantly. All other tested metals did not have any pronounced effect on the SPR band of ACR-AgNPs. The interaction of Hg^{2+} with ACR-AgNPs can be monitored by several factors like surface modification, aggregate morphology, particle size, and shape [43].

Furthermore, sensitivity of ACR-AgNPs for Hg^{2+} was checked in the presence of other metal ions viz. NH_4^+ , Mn^{2+} , Ni^{2+} , Ba^{2+} , Mg^{2+} , Cr^{3+} , Pb^{2+} , Pd^{2+} , Al^{3+} , Sn^{2+} , Fe^{2+} , Co^{2+} , Cu^{2+} , Fe^{3+} , Cd^{2+} , and Hg^{2+} by adding ACR-AgNPs and Hg^{2+} along with all the aforementioned metals. The change in the absorption intensity of ACR-AgNPs+ Hg^{2+} upon addition of various other competing metal ions was recorded and compared with the intensity obtained of the same without interferent. The presence of other metal ions has no significant effect on the quenching of SPR band as obtained for the same amount of mercury without interferent, Figure 7. This indicates that the proposed sensor has efficiently detects the Hg^{2+} ions in the real sample even in the presence of other metal ions.

In order to determine stoichiometry of ACR-AgNPs and Hg^{2+} , Job's method was used in which total concentration was kept constant, while mole fraction of Hg^{2+} was increased gradually from 0.1–1. Values of absorption intensities at 410 nm revealed that minimum absorbance was obtained at mole fraction value of 0.6, indicating 1:1 binding ratio of ACR-AgNPs with Hg^{2+} (Figure 8).

In addition, sensing behavior of synthesized nanosensor at elevated concentration of Hg^{2+} was checked between

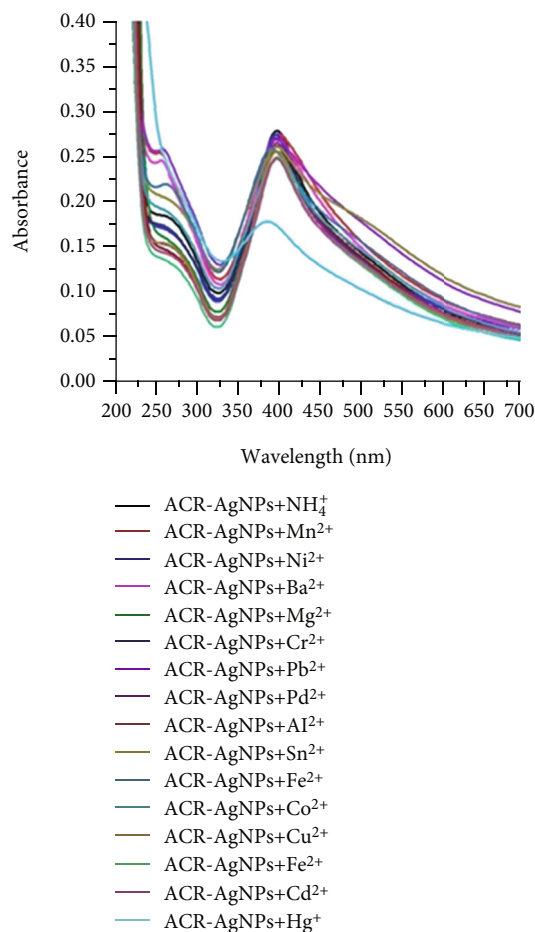


FIGURE 6: Change in the absorption intensity of ACR-AgNPs upon addition of different metal cations (100 μM).

ranges of 5-100 μM Hg^{2+} solutions (Figure 9). An efficient and concentration-dependent decrease in the absorbance intensity of ACR-AgNPs is observed. A linear relation was observed with the increasing concentration of mercury with R^2 value of 0.9893. The limit of detection for mercury ion was found to be 1.65 μM .

3.5. Characterization of ACR-AgNP- Hg^{2+} Complex. The morphology and size of ACR-AgNPs and Hg^{2+} complex were observed through AFM and DLS and SEM (Figure 10). Images obtained through AFM and SEM showed spherical and large size particles. Percent intensity of Hg^{2+} complex of ACR-AgNPs indicated increment in particle size from 40 to 90 nm with a polydispersity index (PDI) of 0.577. Moreover, analysis through AFM, SEM, and DLS revealed increment in size which confirmed ACR-AgNPs complex formation with Hg^{2+} .

The absorbance bands of ACR-AgNPs complex with Hg^{2+} obtained in the range of 1000–4000 cm^{-1} are 3443, 1614, 1205, and 1138 cm^{-1} (Figure 11). Among these, broad absorbance band at 3443 cm^{-1} is due to the bending vibration of secondary amine (-NH). Whereas Hg^{2+} binding to the nitrogen of aromatic amine and oxygen of hydroxyl results in shifting of this band from 3443 to

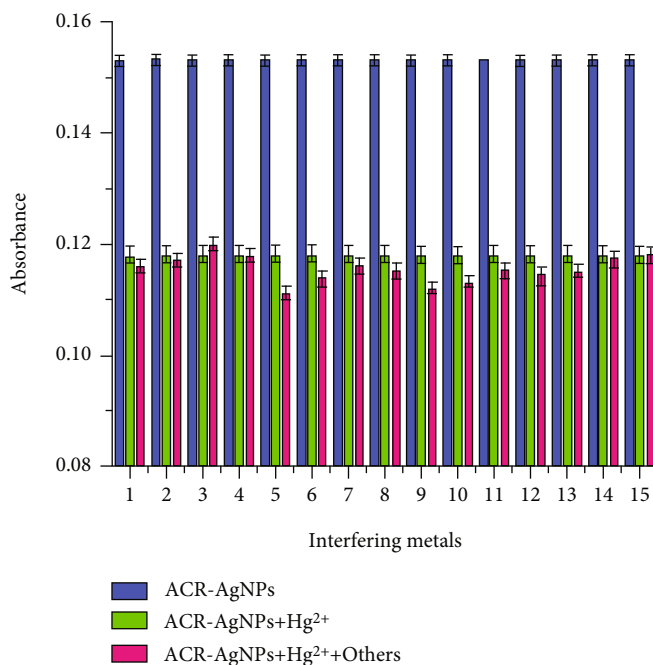


FIGURE 7: Consequence of competing metal ions on the sensing performance of ACR-AgNPs for Hg²⁺, in the presence of 1: NH₄⁺, 2: Mn²⁺, 3: Ni²⁺, 4: Ba²⁺, 5: Mg²⁺, 6: Cr³⁺, 7: Pb²⁺, 8: Pd²⁺, 9: Al³⁺, 10: Sn²⁺, 11: Fe²⁺, 12: Co²⁺, 13: Cu²⁺, 14: Fe³⁺, and 15: Cd²⁺ at 410 nm.

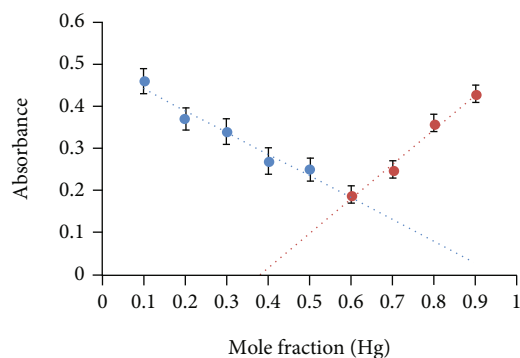


FIGURE 8: Job's plot to observe binding stoichiometry of ACR-AgNPs complex with Hg²⁺.

3580 cm⁻¹ and also decreased broadness of the absorbance band appeared at 3580 cm⁻¹, because in the complex, both amine and hydroxyl groups of ACR-AgNPs are involved in chelation with Hg²⁺. The peak at 1687 cm⁻¹ is due to C=N in ACR-AgNPs and in case of its complex with Hg²⁺, a sharp peak at 1614 cm⁻¹ was observed. Moreover, C-N and C-O-C stretching bands were obtained at 1205 cm⁻¹ and 1138 cm⁻¹ (Figure 11).

It is generally required to evaluate effect of pH on the host guest interaction in a complex in context of real sample applications. To determine an optimized pH for spectroscopic analysis, stability of ACR-AgNPs complex with Hg²⁺ in the pH range of 2-13 is evaluated (Figure 12). To maintain the pH of solutions, the dilute sodium hydroxide and hydrochloric acid was added drop wise.

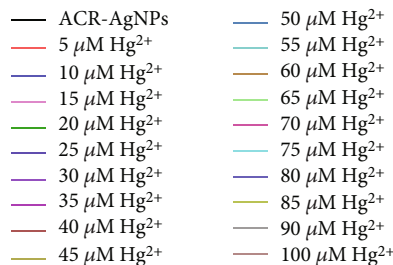
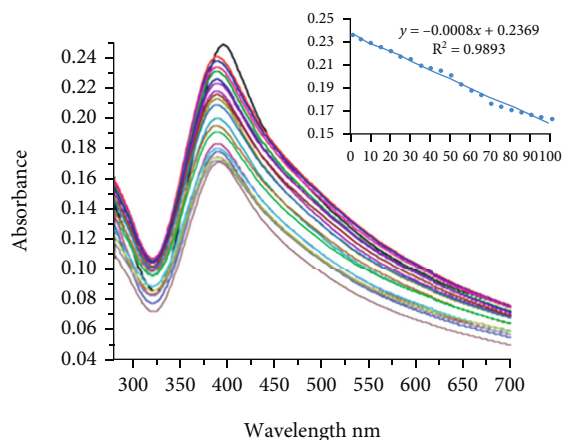


FIGURE 9: Change in the absorption intensity of ACR-AgNPs upon addition of varied concentrations of Hg²⁺ (5-100 μM).

At pH range of 2-6, the decrease in intensity of the ACR-AgNPs complex with Hg²⁺ might be associated with deprotonation of ACR-AgNPs. Conversely, the absorption intensity of ACR-AgNPs complex with Hg²⁺ remained

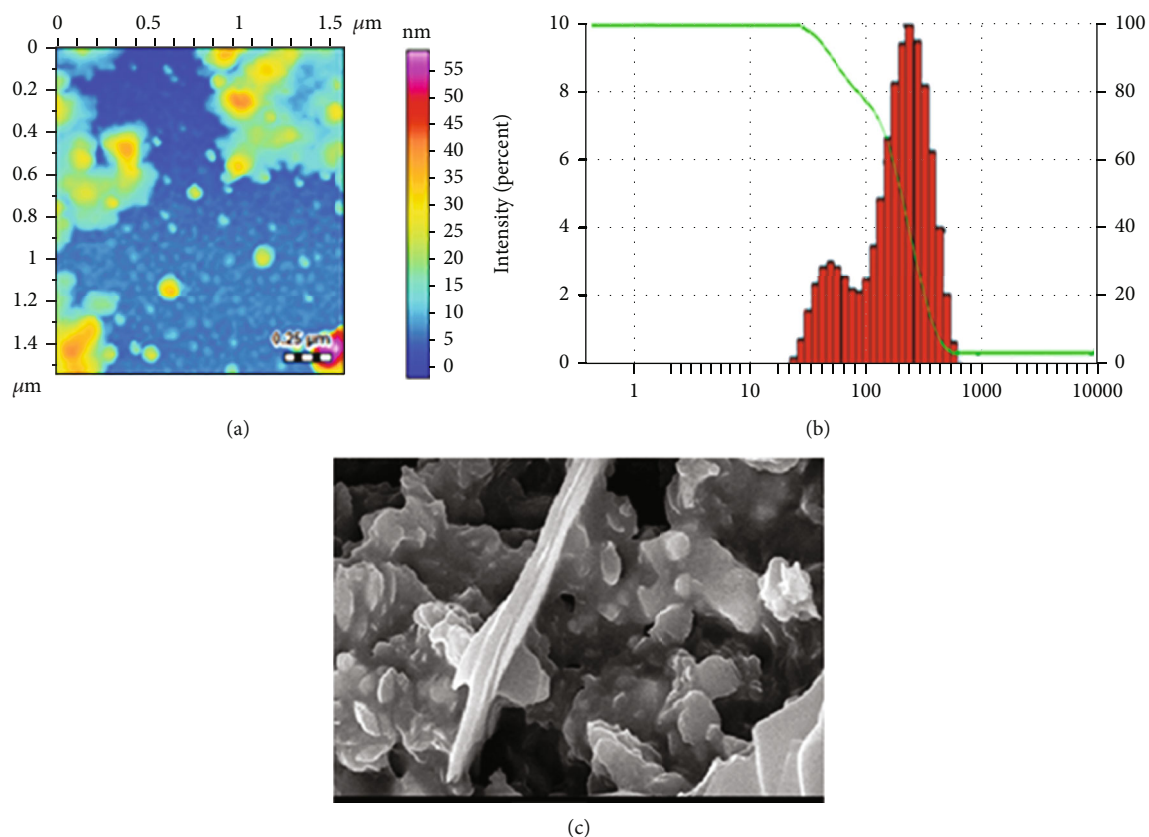


FIGURE 10: Change in surface morphology and size of ACR-AgNPs upon complex formation with Hg²⁺. (a) AFM image of ACR-AgNPs-Hg²⁺. (b) Change in particle size of ACR-AgNPs upon addition of Hg²⁺. (c) SEM image of ACR-AgNPs-Hg²⁺.

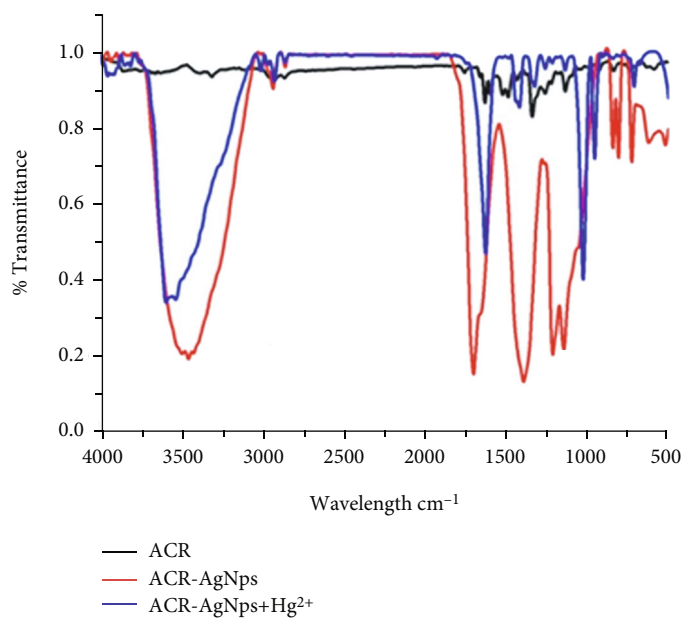


FIGURE 11: FTIR spectra of ACR, ACR-AgNPs, and ACR-AgNPs complex with Hg²⁺.

constant in a pH range of 6-8 followed by a slight decrease in the range of pH 8-10. Furthermore, absorption intensity of the ACR-AgNPs complex with Hg²⁺ increased

in the pH range of 10-14, which may be attributed to the enhancement of nucleophilic character of the donor atoms that facilitate hydrogen bonding. The results

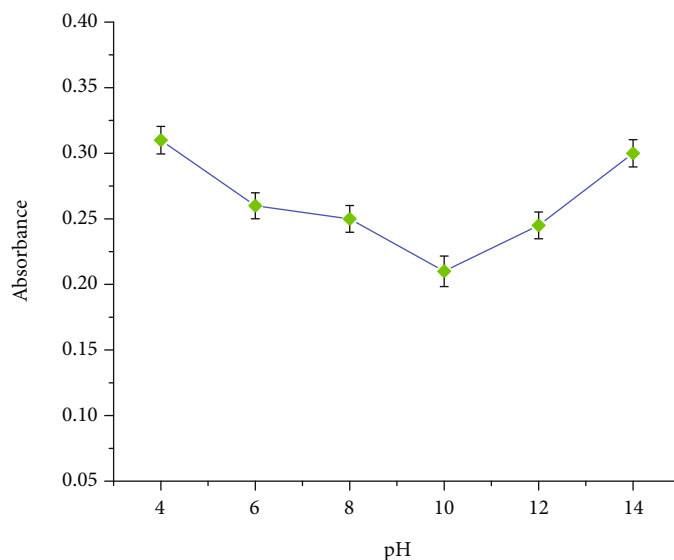


FIGURE 12: Stability of ACR-AgNPs complex with Hg^{2+} in the pH range of 1-14.

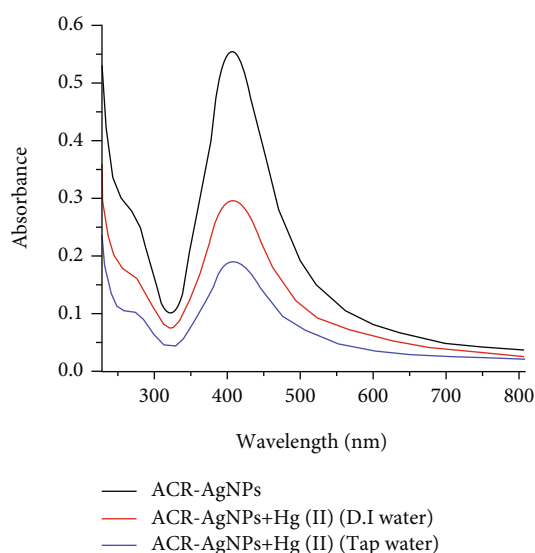


FIGURE 13: Application of ACR-AgNPs for the detection of Hg^{2+} in water sample.

indicate the effectiveness of the ACR-AgNP-based sensor for Hg^{2+} in the whole pH range.

3.6. Detection of Hg^{2+} in Tap Water. To assess the capacity of ACR-AgNPs as nanosensor for Hg^{2+} in water sample, two different Hg^{2+} solutions had been prepared in tap water and deionized water (collected from University of Karachi, Pakistan), respectively. It was noticed that the existence of electrolyte did not alter the absorption spectra and quenching observed by adding nanosensor in mercury (Hg^{2+} ions) solution made up in either deionized water or in laboratory tap water (Figure 13). Similar suppressions are recorded in the intensity of ACR-AgNPs after the addition of mercury in both deionized water and tap water. The percentage recovery of the spiked samples is

TABLE 1: Results for the detection of Hg^{2+} in D.I water and tap water samples (mean \pm SD, $n = 3$).

Samples	S. no	Added conc (μM)	Found conc (μM)	Recovery %	RSD %
D.I water	1	5	4.92 ± 0.23	98.4	1.6
	2	10	9.42 ± 0.13	94.2	1.4
	3	15	14.52 ± 0.09	96.8	2.5
Tap water	1	5	5.12 ± 0.08	102.4	2.3
	2	10	9.94 ± 0.11	99.4	0.9
	3	15	15.35 ± 0.13	102.3	1.4

in the range of 94.2-102.4 as depicted in Table 1. The results illustrate that ACR-AgNPs can be used as a nanosensor for the selective detection of Hg^{2+} in tap water sample.

3.7. Comparison with Other Studies. Up till now, several analytical methods are reported in the literature for the selective detection of Hg^{2+} . Most of the reported methods to detect the mercury (Hg^{2+} ions) in the biological system and aqueous media are difficult, tedious, and costly, Table 2. As can be seen in the Table that the limit of detection of the instrumental methods is lower compared to current method. However, these methods are based on the expensive instruments and time-consuming analysis protocols. The method proposed in this study is based on UV-visible spectroscopy which is easy, economical without any need of an expert. Furthermore, the material used for the synthesis of ACR-AgNPs is cheaper compared. The method is swift, on-spot, and works well for real samples (water samples and biological system).

TABLE 2: Comparison method for the detection of Hg^{2+} ions in tap water.

Techniques	Stabilizing agent	LOD	Reference
Fluorescence	DNA-scaffolded silver nanoclusters	$2.4 \times 10^{-5} \mu\text{M}$	[44]
Colorimetric sensing	Polymer matrix type chitosan matrix nanocomposite	$7.2 \times 10^{-3} \mu\text{M}$	[45]
Fluorescence	Tryptophan stabilized fluorescent Ag nanoclusters	$6.58 \times 10^{-7} \mu\text{M}$	[46]
Fluorometric turn-on and colorimetric detection	Poly(acrylic acid)-templated silver nanoclusters	$2 \times 10^{-3} \mu\text{M}$	[47]
Fluorescence	DNA/AgNC probe	$2.1 \times 10^{-3} \mu\text{M}$	[48]
Electrochemiluminescence	Oligonucleotide	$2 \times 10^{-2} \mu\text{M}$	[49]
UV-visible spectroscopy	Silver nanoparticles	$1.65 \mu\text{M}$	This study

4. Conclusion

Acridine-based conjugated silver nanoparticles showed effective and sensitive method for the detection of Hg^{2+} ions in the real water sample, and these nanoparticles also showed environmentally friendly behaviors. The addition of Hg^{2+} ions prepared in the tap water with solution of silver nanoparticles of nanosensor (ACR-AgNPs) presents a significance decrease in the absorption intensity. The silver nanoparticles of acridine showed selectivity even in the presence of different metals ions and also exhibit significant stability in acidic and basic environment. The presence of electrolyte does not show any disturbance on the absorption intensity of the conjugated silver nanoparticles of acridine. Therefore, these results illustrate that derivative of acridine can be used as an efficient sensors for the detection of environmental pollutants. The limit of detection of proposed sensor obtained from experimental data is $1.65 \mu\text{M}$. The percentage recovery of the spiked samples was in the range of 94.2-102.4%. All the above results show that the nanosensor could be used for the selective detection of mercury in the laboratory tap water and in biological samples.

Data Availability

All the data is presented in the manuscript.

Conflicts of Interest

The authors declare that they have no conflicts of interest.

Acknowledgments

We are thankful to Higher Education Commission, Islamabad, Pakistan, for partial financial support under "National Research Program for Universities" with project number 5743 and International Center for Chemical and Biological Sciences (ICCBS), University of Karachi, Pakistan, for providing lab facilities.

References

- [1] L. Chen, X. Fu, W. Lu, and L. Chen, "Highly sensitive and selective colorimetric sensing of Hg^{2+} based on the morphology transition of silver nanoprisms," *ACS Applied Materials & Interfaces*, vol. 5, pp. 284–290, 2013.
- [2] M. Li, Q. Wang, X. Shi, L. A. Hornak, and N. Wu, "Detection of mercury (ii) by quantum dot/DNA/gold nanoparticle ensemble based nanosensor via nanometal surface energy transfer," *Analytical Chemistry*, vol. 83, no. 18, pp. 7061–7065, 2011.
- [3] X. Niu, Y. Ding, C. Chen, H. Zhao, and M. Lan, "A novel electrochemical biosensor for Hg^{2+} determination based on Hg^{2+} -induced DNA hybridization," *Sensors and Actuators B: Chemical*, vol. 158, no. 1, pp. 383–387, 2011.
- [4] P. Grandjean and P. J. Landrigan, "Developmental neurotoxicity of industrial chemicals," *Lancet*, vol. 368, no. 9553, pp. 2167–2178, 2006.
- [5] C. M. Carvalho, E.-H. Chew, S. I. Hashemy, J. Lu, and A. Holmgren, "Inhibition of the Human Thioredoxin System: a molecular mechanism of mercury toxicity*," *The Journal of Biological Chemistry*, vol. 283, no. 18, pp. 11913–11923, 2008.
- [6] T. W. Clarkson, L. Magos, and G. J. Myers, "The toxicology of mercury—current exposures and clinical manifestations," *New England Journal of Medicine*, vol. 349, no. 18, pp. 1731–1737, 2003.
- [7] B. Gu, L. Huang, N. Mi et al., "An esipt-based fluorescent probe for highly selective and ratiometric detection of mercury (ii) in solution and in cells," *Analyst*, vol. 140, no. 8, pp. 2778–2784, 2015.
- [8] H. Louie, C. Wong, Y. J. Huang, and S. Fredrickson, "A study of techniques for the preservation of mercury and other trace elements in water for analysis by inductively coupled plasma mass spectrometry (icp-ms)," *Analytical Methods*, vol. 4, no. 2, pp. 522–529, 2012.
- [9] S. M. Gustin, M. Coolbaugh, M. Engle et al., "Atmospheric mercury emissions from mine wastes and surrounding geologically enriched terrains," *Environmental Geology*, vol. 43, no. 3, pp. 339–351, 2003.
- [10] Y. Chen, H. Zhao, Z. Xie, H. Huang, S. Zang, and B. Lian, "Heavy metal pollution characteristics in the Kaili coal mining region, Guizhou province, China," *Journal of Residuals Science and Technology*, vol. 12, pp. 123–131, 2015.
- [11] L. B. Escudero, R. A. Olsina, and R. G. Wuilloud, "Polymer-supported ionic liquid solid phase extraction for trace inorganic and organic mercury determination in water samples by flow injection-cold vapor atomic absorption spectrometry," *Talanta*, vol. 116, pp. 133–140, 2013.
- [12] A. T. Reis, C. B. Lopes, C. M. Davidson, A. C. Duarte, and E. Pereira, "Extraction of mercury water-soluble fraction from soils: an optimization study," *Geoderma*, vol. 213, pp. 255–260, 2014.

- [13] G. N. George, S. P. Singh, G. J. Myers, G. E. Watson, and I. J. Pickering, "The chemical forms of mercury in human hair: a study using x-ray absorption spectroscopy," *Journal of Biological Inorganic Chemistry*, vol. 15, no. 5, pp. 709–715, 2010.
- [14] H. Tan, Y. Zhang, and Y. Chen, "Detection of mercury ions (Hg^{2+}) in urine using a terbium chelate fluorescent probe," *Sensors and Actuators B: Chemical*, vol. 156, no. 1, pp. 120–125, 2011.
- [15] H. N. Kim, W. X. Ren, J. S. Kim, and J. Yoon, "Fluorescent and colorimetric sensors for detection of lead, cadmium, and mercury ions," *Chemical Society Reviews*, vol. 41, no. 8, pp. 3210–3244, 2012.
- [16] J. S. Lee, M. S. Han, and C. A. Mirkin, "Colorimetric detection of mercuric ion (Hg_2^+) in aqueous media using DNA-functionalized gold nanoparticles," *Angewandte Chemie International Edition*, vol. 46, no. 22, pp. 4093–4096, 2007.
- [17] X. Xue, F. Wang, and X. Liu, "One-step, room temperature, colorimetric detection of mercury (Hg_2^+) using DNA/nanoparticle conjugates," *Journal of the American Chemical Society*, vol. 130, no. 11, pp. 3244–3245, 2008.
- [18] L. Chen, J. Li, and L. Chen, "Colorimetric detection of mercury species based on functionalized gold nanoparticles," *ACS Applied Materials & Interfaces*, vol. 6, no. 18, pp. 15897–15904, 2014.
- [19] Y. Wang, F. Yang, and X. Yang, "Colorimetric detection of mercury (ii) ion using unmodified silver nanoparticles and mercury-specific oligonucleotides," *ACS Applied Materials & Interfaces*, vol. 2, no. 2, pp. 339–342, 2010.
- [20] J. H. An, S. J. Park, O. S. Kwon, J. Bae, and J. Jang, "High-performance flexible graphene aptasensor for mercury detection in mussels," *ACS Nano*, vol. 7, no. 12, pp. 10563–10571, 2013.
- [21] G. Zhang, D. Zhang, S. Yin, X. Yang, Z. Shuai, and D. Zhu, "1,3-Dithiole-2-thione derivatives featuring an anthracene unit: new selective chemodosimeters for hg (ii) ion," *Chemical Communications*, vol. 41, no. 16, pp. 2161–2163, 2005.
- [22] J. O. Moon, M. G. Choi, T. Sun, J.-I. Choe, and S.-K. Chang, "Synthesis of thionaphthalimides and their dual Hg_2^+ -selective signaling by desulfurization of thioimides," *Dyes and Pigments*, vol. 96, no. 1, pp. 170–175, 2013.
- [23] Y. Li, N. Liu, H. Liu et al., "A novel label-free fluorescence assay for one-step sensitive detection of Hg_2^+ in environmental drinking water samples," *Scientific Reports*, vol. 7, no. 1, p. 45974, 2017.
- [24] K. Chen, S. She, J. Zhang, A. Bayaguud, and Y. Wei, "Label-free colorimetric detection of mercury via Hg_2^+ ions-accelerated structural transformation of nanoscale metal-oxo clusters," *Scientific Reports*, vol. 5, no. 1, article 16316, 2015.
- [25] C. J. Kirubakaran, D. Kalpana, Y. S. Lee et al., "Biomediated silver nanoparticles for the highly selective copper (ii) ion sensor applications," *Industrial and Engineering Chemistry Research*, vol. 51, no. 21, pp. 7441–7446, 2012.
- [26] C. K. Tagad, S. R. Dugasani, R. Aiyer, S. Park, A. Kulkarni, and S. Sabharwal, "Green synthesis of silver nanoparticles and their application for the development of optical fiber based hydrogen peroxide sensor," *Sensors and Actuators B: Chemical*, vol. 183, pp. 144–149, 2013.
- [27] W. Lian, S. Liu, J. Yu et al., "Electrochemical sensor using neomycin-imprinted film as recognition element based on chitosan-silver nanoparticles/graphene-multiwalled carbon nanotubes composites modified electrode," *Biosensors & Bioelectronics*, vol. 44, pp. 70–76, 2013.
- [28] M. Bindhu and M. Umadevi, "Antibacterial and catalytic activities of green synthesized silver nanoparticles," *Spectrochimica Acta Part A: Molecular and Biomolecular Spectroscopy*, vol. 135, pp. 373–378, 2015.
- [29] S. M. Pourmortazavi, M. Taghdiri, V. Makari, and M. Rahimi-Nasrabadi, "Procedure optimization for green synthesis of silver nanoparticles by aqueous extract of eucalyptus oleosa," *Spectrochimica Acta Part A: Molecular and Biomolecular Spectroscopy*, vol. 136, pp. 1249–1254, 2015.
- [30] P. R. Sre, M. Reka, R. Poovazhagi, M. A. Kumar, and K. Murugesan, "Antibacterial and cytotoxic effect of biologically synthesized silver nanoparticles using aqueous root extract of *Erythrina indica lam*," *Spectrochimica Acta Part A: Molecular and Biomolecular Spectroscopy*, vol. 135, pp. 1137–1144, 2015.
- [31] S. Ahmed, Saifullah, M. Ahmad, B. L. Swami, and S. Ikram, "Green synthesis of silver nanoparticles using *Azadirachta indica* aqueous leaf extract," *Journal of Radiation Research and Applied Science*, vol. 9, no. 1, pp. 1–7, 2016.
- [32] M. Pattanayak and P. Nayak, "Green synthesis and characterization of zero valent iron nanoparticles from the leaf extract of *azadirachta indica* (neem)," *World Journal of Nano Science & Technology*, vol. 2, pp. 06–09, 2013.
- [33] J. Mittal, A. Batra, A. Singh, and M. M. Sharma, "Phytofabrication of nanoparticles through plant as nanofactories," *Advances in Natural Sciences: Nanoscience and Nanotechnology*, vol. 5, no. 4, article 043002, 2014.
- [34] W. Rungratanawanich, G. Cenini, A. Mastinu et al., "T-oryzanol improves cognitive function and modulates hippocampal proteome in mice," *Nutrients*, vol. 11, no. 4, p. 753, 2019.
- [35] A. Kumar, M. Memo, and A. Mastinu, "Plant behaviour: an evolutionary response to the environment?," *Plant Biology*, vol. 22, no. 6, pp. 961–970, 2020.
- [36] M. M. Patel, M. D. Mali, and S. K. Patel, "Bernthsen synthesis, antimicrobial activities and cytotoxicity of acridine derivatives," *Bioorganic & Medicinal Chemistry Letters*, vol. 20, no. 21, pp. 6324–6326, 2010.
- [37] W. A. Denny, "Chemotherapeutic effects of acridine derivatives," *Medicinal Chemistry Reviews Online*, vol. 1, no. 3, pp. 257–266, 2004.
- [38] M. Galdino-Pitta, M. Pitta, M. Lima, L. Galdino, and R. Pitta, "Niche for acridine derivatives in anticancer therapy," *Mini Reviews in Medicinal Chemistry*, vol. 13, no. 9, pp. 1256–1271, 2013.
- [39] B. Zhang, X. Li, B. Li, C. Gao, and Y. Jiang, "Acridine and its derivatives: a patent review (2009–2013)," *Expert Opinion on Therapeutic Patents*, vol. 24, no. 6, pp. 647–664, 2014.
- [40] I. O. Isaac, M. Al-Rashida, S. U. Rahman et al., "Acridine-based (thio) semicarbazones and hydrazones: synthesis, in vitro urease inhibition, molecular docking and in-silico adme evaluation," *Bioorganic Chemistry*, vol. 82, pp. 6–16, 2019.
- [41] S. M. Shaban, I. Aiad, M. M. El-Sukkary, E. Soliman, and M. Y. El-Awady, "Synthesis of newly cationic surfactant based on dimethylaminopropyl amine and their silver nanoparticles: characterization; surface activity and biological activity," *Chinese Chemical Letters*, vol. 28, no. 2, pp. 264–273, 2017.
- [42] N. A. Begum, S. Mondal, S. Basu, R. A. Laskar, and D. Mandal, "Biogenic synthesis of au and ag nanoparticles using aqueous solutions of black tea leaf extracts," *Colloids and Surfaces B: Biointerfaces*, vol. 71, no. 1, pp. 113–118, 2009.

- [43] J. N. Anker, W. P. Hall, O. Lyandres, N. C. Shah, J. Zhao, and R. P. Van Duyne, "Biosensing with plasmonic nanosensors," in *Nanoscience and technology: A Collection of Reviews from Nature Journals*, pp. 308–319, Nature Publishing Group, 2009.
- [44] M. Xu, Z. Gao, Q. Wei, G. Chen, and D. Tang, "Label-free hairpin DNA-scaffolded silver nanoclusters for fluorescent detection of Hg²⁺ using exonuclease iii-assisted target recycling amplification," *Biosensors & Bioelectronics*, vol. 79, pp. 411–415, 2016.
- [45] E. Nivethaa, V. Narayanan, and A. Stephen, "Synthesis and spectral characterization of silver embedded chitosan matrix nanocomposite for the selective colorimetric sensing of toxic mercury," *Spectrochimica Acta Part A: Molecular and Biomolecular Spectroscopy*, vol. 143, pp. 242–250, 2015.
- [46] P. Bian, L. Xing, Z. Liu, and Z. Ma, "Functionalized-tryptophan stabilized fluorescent ag nanoclusters: synthesis and its application as Hg²⁺ ions sensor," *Sensors and Actuators B: Chemical*, vol. 203, pp. 252–257, 2014.
- [47] Y. Tao, Y. Lin, Z. Huang, J. Ren, and X. Qu, "Poly (acrylic acid)-templated silver nanoclusters as a platform for dual fluorometric turn-on and colorimetric detection of mercury (ii) ions," *Talanta*, vol. 88, pp. 290–294, 2012.
- [48] J. Peng, J. Ling, X.-Q. Zhang et al., "Sensitive detection of mercury and copper ions by fluorescent DNA/ag nanoclusters in guanine-rich DNA hybridization," *Spectrochimica Acta Part A: Molecular and Biomolecular Spectroscopy*, vol. 137, pp. 1250–1257, 2015.
- [49] M. Zhang, L. Ge, S. Ge et al., "Three-dimensional paper-based electrochemiluminescence device for simultaneous detection of Pb²⁺ and Hg²⁺ based on potential-control technique," *Biosensors & Bioelectronics*, vol. 41, pp. 544–550, 2013.